sciendo

POLISH MARITIME RESEARCH 1 (117) 2023 Vol. 30; pp. 65-77
10.2478/pomr-2023-0007

EXPERIMENTAL STUDY ON VIBRATION OF A ROTATING PIPE IN STILL WATER AND IN FLOW

Xinge Geng [1]
Weiguo Wu [2]
Erpeng Liu [1]
Yongshui Lin [1]
Wei Chen *[3]
Chang-Kyu Rheem [4]

[1] Hubei Key Laboratory of Theory and Application of Advanced Materials Mechanics, Department of Mechanics and Engineering Structure, Wuhan University of Technology, Wuhan, China
[2] Green & Smart River-Sea-Going Ship Cruise and Yacht Research Center, Wuhan University of Technology, Wuhan, China
[3] School of Naval Architecture, Ocean and Energy Power Engineering, Wuhan University of Technology, Wuhan, China
[4] Department of Ocean Technology, Policy and Environment, The University of Tokyo, Tokyo, Japan

* Corresponding author: *whutcw01@126.com (Wei Chen)*

ABSTRACT

To illustrate the vibration characteristics of a rotating pipe in flow, experiments were conducted for a pipe in flow, a rotating pipe in still water and a rotating pipe in flow. For the pipe in flow without rotation, the trajectory diagram is '8' shaped. For the rotating pipe in still water, a multiple frequency component was induced, and a 'positive direction whirl' was found. For the flow and rotation, at a flow velocity of 0.46 m/s, the vibration is dominated by the combination of flow and rotation. With an increase in rotating frequency, the trajectory of the rotating pipe varies from an '8' shape to a circular shape and the 'reverse direction whirl' is induced, which is different from 'positive direction' in still water. The vibration frequency ratio increases uniformly with flow velocity. At a flow velocity of 1.02 m/s, at which the frequency is close to the theoretical natural frequency, the vibration frequency ratio is f≈1. Predominantly governed by vortex-induced vibration (VIV), the vibration behavior of a rotating pipe subjected to fluid flow conditions has been found to exhibit complete vanishing of whirl. The vibration characteristics of a rotating pipe in flow are studied by the experiments which is benefit for structural drilling design.*

Keywords: flow-induced vibration; rotating pipe; vibration frequency; whirl; VIV

INTRODUCTION

Riserless drilling is significant for ocean exploration [1-3]. As the core component of riserless drilling, under flow and rotation, flow-induced vibration seems to increase the damage to the drilling pipe, and the phenomenon of flow-induced vibration of the drilling pipe has attracted extensive attention from scholars [4-7].

As the basic model of a drilling pipe, the investigation of hydrodynamics and wake of a rotating cylinder has been conducted by many researchers. When a cylinder rotates in flow, it causes an asymmetric wake behind it due to the Magnus effect. For the rotating cylinder in flow, studies of the wake concerned with rotation rate, have been conducted [8]. It was found that, when the rotation rate $\alpha < 2$, the shedding vortex was similar to that of the Carmen vortex street [9]. When the rotation rate $\alpha > 2$, the shedding vortex behind the rotating cylinder is suppressed [10]. Furthermore, hydrodynamic studies under different rotation rates and Reynolds numbers have been conducted. Ray et al. [11, 12] conducted numerical and experimental analysis of the bypass flow of a rotating cylinder, at Reynolds numbers from 5000-11800. They summarised the variation of lift and drag coefficients and analysed the flow field characteristics

behind the rotating cylinder. Chew et al. [13] simulated the flow around a rotating cylinder when Re = 1000 and $0 \le \alpha \le 6$, and predicted that the lift coefficient was 9.1 when $\alpha = 6$. They considered that the Prandtl limit could not be exceeded. A significant amount of research has been published with regards to identifying the shedding regimes of flow past a rotating cylinder. Stojkovi et al. [9, 14] found that a second vortex shedding regime exists when the rotation rate increases. For the second shedding regime, the amplitudes of the lift and drag coefficients are much larger than those characterising the first shedding regime; they sometimes generate negative values for the mean drag, i.e. generating mean thrust. According to the first and second shedding regime, there are three critical rotation rates [15-17].

Furthermore, many studies have been conducted concerning a spring-mounted rotating cylinder in flow. Ding et al. [18] conducted a numerical simulation of the eddy current-induced vibrations in a rigid cylinder rotating counter-clockwise with a reduced velocity of $3 \le U^* \le 12$. The Magnus effect caused by rotation enlarges the offset from the initial position of the rotating cylinder. The movement trajectory of the non-rotating cylinder in the shear flow presents a droplet-shape, which is obviously different from the '8' shaped trajectory of uniform flow. Zou et al. [19, 20] numerically studied the flow-induced vibration of a rotating cylinder in the reduced velocity range of $3 \le U^* \le 14$. The rotating cylinder can vibrate freely in the flow and cross-flow directions. The effect of rotation on flow-induced vibration (FIV) is understood by analysing the amplitude and frequency. The oscillations of the cylinder are significantly enhanced by rotation in the flow direction but the opposite phenomenon is observed in the cross-flow direction. Munir et al. [21, 22] found that at Reynolds numbers of 100 to 200, the transition from a two-dimensional vortex shedding mode to a vortex-free shedding mode occurs when the rotation rate is increased beyond a critical value. Further increases in the rotation rate lead to a transition to three-dimensional flow. It is found that the VIV is suppressed when the rotation rate exceeds a critical value, which is dependent on the reduced velocity. For a constant reduced velocity, the amplitude of the vibration is found to increase with increasing rotation rate until the latter reaches its critical value for VIV suppression, beyond which the vibration amplitude becomes extremely small. If the rotation rate is greater than its critical value, vortex shedding ceases and hairpin vortices are observed due to the rotation of the cylinder. Tang et al. [23] organised the rotating cylinders into four response modes for the existing research: active rotation, passive rotation, and a co-existence of rotation and FIV. For the active rotation response, factors including the Reynolds number, rotation speed and frequency, and the influence of FIV occurrence, were investigated.

To study the vibration characteristics and flow characteristics of rotating cylinders in flow, some scholars have experimentally studied elastically mounted rotating circular cylinders. Zhao et al. [24] experimentally studied the online flow-induced vibration of an elastically mounted cylinder under forced rotation in flow. The experiments characterise the structural vibration, fluid forces and wake structure of the fluid-structure system at a low mass ratio (the ratio of the total mass to the displaced fluid mass), over a wide parameter space spanning the reduced velocity range $5 \le U^* \le 32$ and the rotation rate range $3 \le \alpha \le 14$. This suggests that the mechanism for sustaining the large rotation-induced galloping oscillations at higher values of α, is due to a combination of dynamic forcing from the locked induced vortex shedding (associated with the oscillations) and dynamic forcing evaluated using quasi-steady theory. Wong et al. [25] studied the flow-induced vibration (FIV) of an elastically mounted cylinder at a forced rotational oscillation frequency ratio $0 \le f_r^* \le 4{,}5$ and a forced rotational velocity ratio $3 \le \alpha_r^* \le 14$. New wake modes were identified in the rotary lock-on and tertiary lock-on regions using particle image velocimetry measurements at selected points in the f_r^* - α_r^* parameter space.

The study of rotating cylinders in flow is mainly supported by elasticity, both in numerical simulations and experimental studies [21, 25-28]. Indeed, the drilling pipe is flexible and freely supported rotating pipe experiments are deficient, which is significant when illustrating the vibration behaviour of the drilling pipe in flow. In this paper, an experimental method for the vibration of a free-rotating pipe in flow is proposed and the related experimental equipment is designed. The analysis of rotating pipe vibration under the combined action of flow and rotation is carried out. The vibration data of the rotating pipe is extracted through image tracking technology and coordinate conversion. The displacements, motion trajectories, and vibration frequencies of rotating pipes are compared and analysed, and the vibration characteristics of the rotating pipe under the combined action of water flow and rotation are obtained.

METHOD

EXPERIMENTAL DEVICE

The experimental device is shown in Fig. 1. The rotating pipe was mainly composed of upper and lower hollow shaft parts, unplasticized polyvinyl chloride(UPVC) pipe parts (experimental components) and connectors. The upper and lower couplings were used to fix the UPVC pipe and transmit the torque of the motor to the UPVC pipe. Based on the segmented design of the rotating pipe model, the different parts were connected by couplings which improve the uniformity and stability of torque transmission. A 57BYGH245-4504B-ZK20 hollow stepping motor was mainly used to drive the pipe. The model of the motor driver was LK-20504, the model of the controller was DKC-Y110, and the power was 36 V for the system, which can provide a rotation frequency range of 0.0-7.5 Hz. The velocity of flow was measured by a flow meter, the vibration of the rotating pipe was recorded by a high-speed camera, and experimental data was analysed and processed by an acquisition computer.

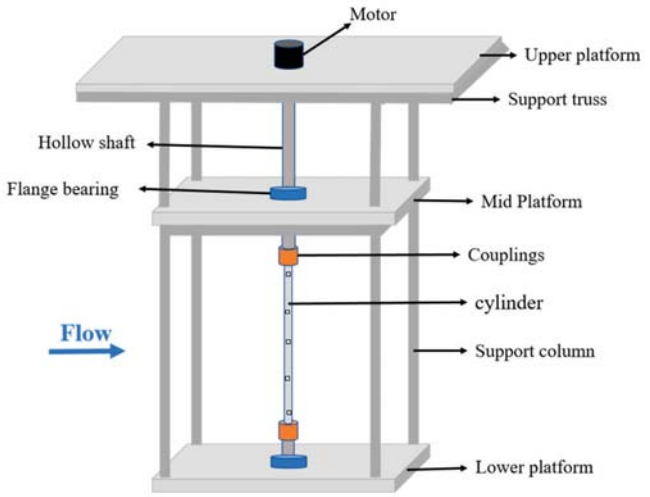

Fig. 1. Schematic diagram of the experimental setup

EXPERIMENTAL PARAMETER DESIGN

To observe the flow-induced vibration response of the rotating pipe, a large aspect ratio *L/D* and lower bending stiffness *EI* are needed for the UPVC pipe. The UPVC pipe was selected with an outer diameter of 12 mm, an inner diameter of 8 mm, and a length-to-diameter ratio of . $L/D \approx 83$. The specific material parameters of the model are shown in Table 1.

Table 1. Material parameters of UPVC rotating pipe model

Material Properties	Parameter
Length (m)	1.0
Outer diameter (m)	0.012
Inner diameter (mm)	0.008
Elastic modulus (Pa)	3.725×10^9
Density (kg/m^3)	1540.0

For the VIV, when the shedding frequency f_s is close to the natural frequency of the rotating pipe f_n, the VIV of the rotating pipe is locked. The shedding frequency *fs* is mainly related to the water flow velocity *U* and the outer diameter *D* of the rotating pipe, which can be expressed by the Strouhal number:

$$f_s = St\frac{U}{D} \tag{1}$$

In the rotating pipe flow-induced vibration experiment, the ends of the rotating pipe are simply supported. The natural frequency can be solved by the following formula:

$$f_n = \beta_n^2\sqrt{\frac{E}{m}} \qquad (n=1,2,3,...) \tag{2}$$

where *n* is the modal order, *E* is the elastic modulus of the rotating pipe, *I* is the moment of inertia of the section, L is the length of the rotating pipe, *m* is the total mass per unit length (where $m = m_s + C_A m_d$), m_s is the mass of the rotating pipe per unit length, m_d is the mass of the water displaced by the rotating pipe per unit length, C_A is the additional mass coefficient (usually, $C_A = 1$), and β_n is the characteristic root of the vibration equation of the clamped beam:

$$\begin{cases} \beta_1 L = 4.730 \\ \beta_n L \approx \left(r+\dfrac{1}{2}\right)\pi \qquad (n=2,\ 3,\ \bullet\ \bullet\ \bullet) \end{cases} \tag{3}$$

Fig. 2 shows the mode shapes and theoretical natural frequencies of rotating pipes for each order.

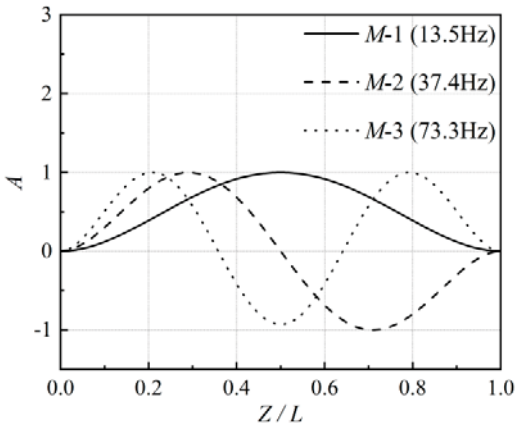

Fig. 2. Mode shape diagram and theoretical natural frequency of drill string for each order

When the shedding frequency f_s is close to the natural frequency f_n of the rotating pipe, the relationship between the VIV response mode and the water flow velocity *U* can be established:

$$U = \frac{D\beta_n^2}{St}\sqrt{\frac{EI}{m}} \quad (n=1,2,3,...) \tag{4}$$

The equation can roughly predict the flow velocity corresponding to each modal response of the rotating pipe.

During the experiment, the velocity of flow was set as U = 0 m/s, 0.46 m/s, 0.72 m/s, and 1.02 m/s. The rotation frequencies were f = 0.0 Hz, 2.5 Hz, 5.0 Hz, and 7.5 Hz. The working condition f = 0.0 Hz , U = 0 m/s was used to calibrate the initial position of the rotating pipe.

EXPERIMENTAL MEASUREMENT METHODS

During the experiment, the velocity of flow was measured by a flow meter. The rotation frequency was driven by the motor and the vibration of the rotating pipe was recorded by a high-speed camera. Both sides of the circulation tank are composed of glass, and two high-speed cameras were used to shoot the same side with a cross angle. Fig. 3 shows the monitoring method used in the experiment.

(*a*)

(*b*)

Fig. 3. Water velocity meter (a) and motion monitoring (b) during the experiment

The schematic diagram of the plane position of the camera is shown in Fig. 4. The parallax angle γ satisfies the equation:

$$y_1 \tan\gamma + y_2 \tan\alpha = x_0 \tag{5}$$

$$\gamma = \arcsin\left(\frac{\sin\alpha}{n}\right) \tag{6}$$

where $n = \dfrac{\sin\alpha}{\sin\gamma} = 1.33$ is the refractive index of water.

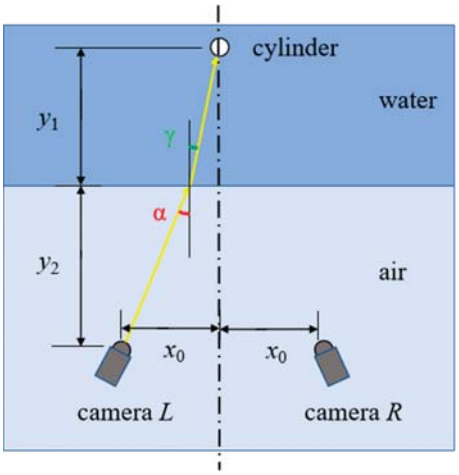

Fig. 4. Schematic diagram of the plane position of the camera

The actual displacement $\triangle x$, $\triangle y$ of the rotating pipe in the *x* and *y* directions satisfies:

$$\Delta L = \Delta x \cos\gamma + \Delta y \sin\gamma \tag{7}$$

$$\Delta R = \Delta x \cos\gamma - \Delta y \sin\gamma \tag{8}$$

where ΔL and ΔR are the displacements of the rotating pipe when the vibration is captured by the left and right cameras.

According to the coordinate transformation, the position of the rotating pipe rotation at each moment and the trajectory map of the rotating pipe can be obtained.

EXPERIMENTAL RESULTS AND ANALYSIS

During the experiments, the flow-induced vibrations of the rotating pipe were observed at rotation frequencies f = 0.0 Hz, 2.5 Hz, 5.0 Hz, and 7.5 Hz at flow velocities U = 0.00 m/s, 0.46 m/s, 0.72 m/s, and 1.02 m/s. The vibration characteristics of the rotating pipe under the combined action of water flow and rotation were obtained.

FLOW EFFECT

For the pipe in flow without rotation, the vibration of the pipe is mainly caused by vortex shedding. Fig. 5 shows the in-line and cross-flow direction displacement time histories and motion trajectories of the middle of the pipe at different flow velocities. The motion shows a certain periodicity. Due to the dragging force, the pipe has a certain offset in the in-line direction, and the offset of the pipe increases with the increase of flow velocity. From the trajectory diagram, it can be seen that the trajectory of the pipe is roughly in the shape of a figure '8', which was similarly observed in the previous study [29]. The shape of the trajectory is more obvious with the increase of flow velocity.

Fig. 6 shows the displacement spectrum of the middle position of the pipe at different velocities. The frequency of the displacement in the in-line direction is twice that of the cross-flow direction, which corresponds to the '8' shape of the displacement trajectory in Fig. 5. With the increase of flow velocity, the frequency in both directions increases. As the '8' shape of the displacement trajectory becomes inclined, twice the frequency component of the vibration in the cross-flow direction is obtained. At a flow velocity of U = 1.02 m/s, one vibration frequency is 12.4 Hz, which is close to the theoretical first-order natural frequency (13.5Hz). The vibration shows a first-order vibration mode and the displacement is much larger than that at other flow velocities, as shown in Fig. 7.

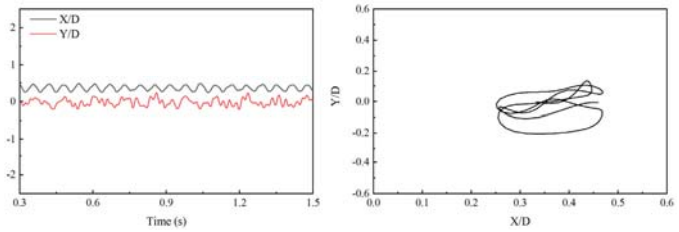

(*a*) $U = 0.46$ m/s

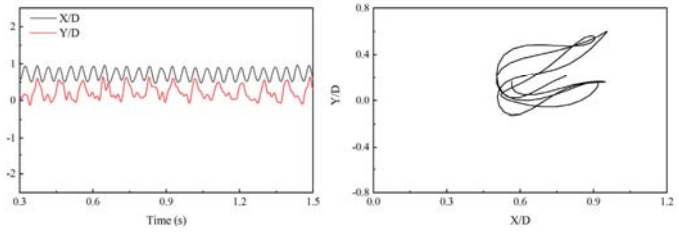

(*b*) $U = 0.72$ m/s

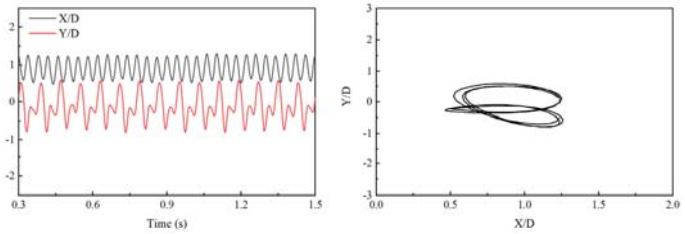

(*c*) $U = 1.02$ m/s

Fig. 5. Time course histories of displacement in the middle of the pipe and trajectories of motion at different velocities

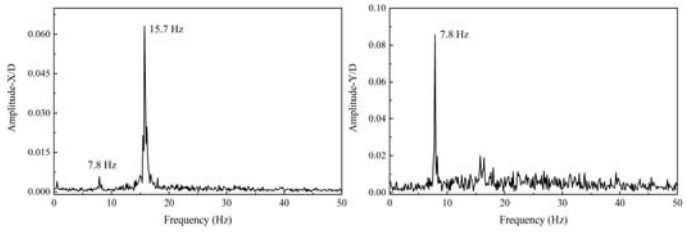

(*a*) $U = 0.46$ m/s

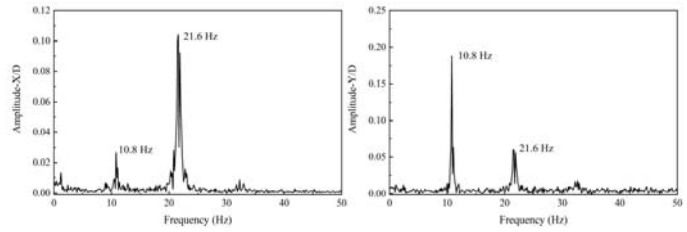

(*b*) $U = 0.72$ m/s

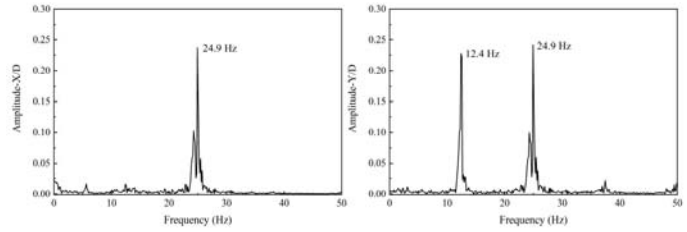

(*c*) $U = 1.02$ m/s

Fig. 6. Spectrum of displacement in the middle of the pipe at different velocitiess

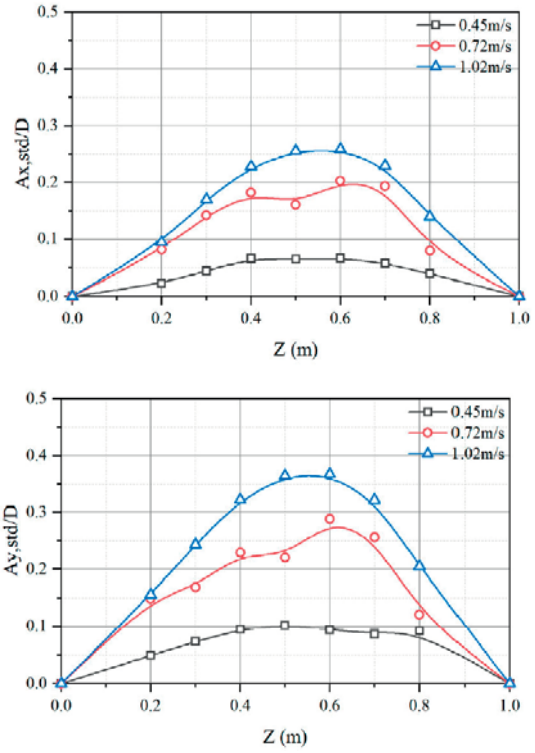

Fig. 7. RMS values of the cross-flow and cross-flow amplitudes of the pipe at different velocities

ROTATION EFFECT

When the pipe rotates in still water, a slight inertial motion around the initial axis (the axis of the initial static equilibrium position) occurs due to the eccentric unbalancing force caused by the rotation, which is termed 'whirl' in previous works [30]. Fig. 8 shows the time histories of the displacement and motion trajectories of the middle position of the pipe at different frequencies. With an increase in rotation frequency, the time history of displacement becomes a standard sinusoidal curve and the motion gradually becomes a circle. In particular, the motion direction is consistent with the rotation direction of the pipe, which can be termed 'positive direction whirl'. The maximum displacement value at a rotating frequency of 7.5 Hz is approximately 0.05 D, which is still much smaller than those induced by flow, as shown in Fig. 7.

As the frequency analysis shows in Fig. 9, without flow, the similarity of the frequency characteristics in the X and Y directions are obtained. The first peak frequency of the whirl is the same as the rotating frequency. Rotational motion induces multiple frequency components, particularly at low rotational frequencies, such that at a rotating frequency of 2.5 Hz, the components of 2.5 Hz, 5 Hz (twice) and 10 Hz (four times) are induced. With an increase in rotating frequency, the first peak frequency of the component gradually becomes close to the theoretical first-order natural frequency, and the components of multiple time frequencies are suppressed.

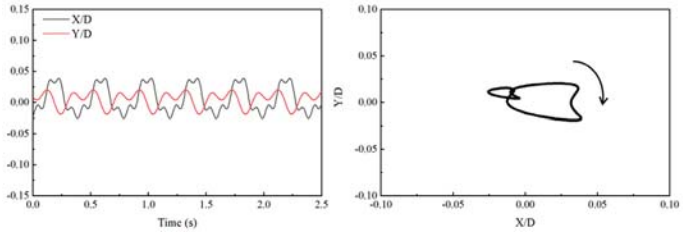

(*a*) $f = 2.5$ Hz

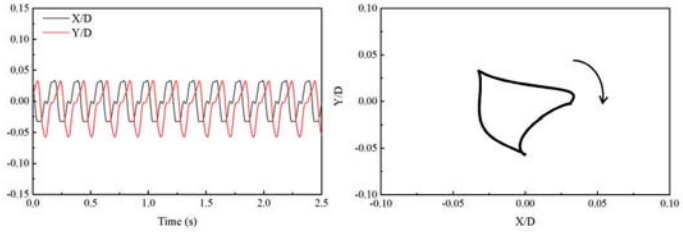

(*b*) $f = 5.0$ Hz

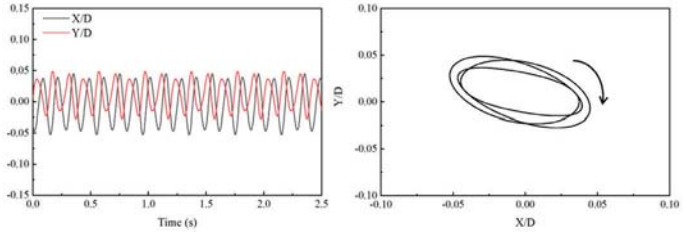

(*c*) $f = 7.5$ Hz

Fig. 8. Time course of displacement at the midpoint of the pipe under different rotation frequencies in still water and the trajectory of the motion

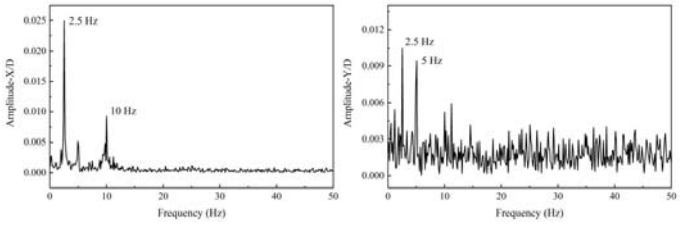

(*a*) $f = 2.5$ Hz

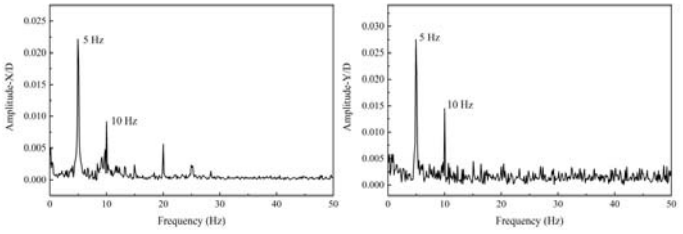

(*b*) $f = 5.0$ Hz

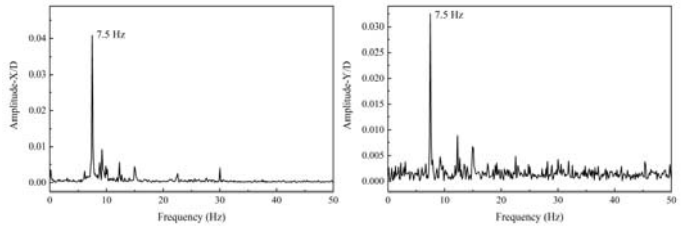

(*c*) $f = 7.5$ Hz

Fig. 9. Frequency spectrum of the midpoint displacement curve of the rotating pipe under different rotation frequencies in still water

EFFECT OF COMBINATION OF FLOW AND ROTATION

Fig. 10 shows the displacement time histories and motion trajectories of the middle of the rotating pipe at different rotation frequencies with a velocity of 0.46 m/s. With an increase in rotation frequency, the cross-flow vibration amplitude gradually increases. The frequency of vibration in the in-line direction is the same as in the cross-flow direction while, in the absence of rotation, the frequency of in-line vibration is twice that of cross-flow vibration. The trajectory gradually varies from the original figure '8' to a circular shape. The direction of motion was opposite to the direction of rotation of the rotating pipe (different from that shown in Fig. 8), and is called the 'reverse direction whirl'.

Fig. 11 shows the displacement spectrum in the middle of the rotating pipe at different rotation frequencies for $U = 0.46$ m/s. Without rotation, the vibration is mainly caused by VIV, with the dominant frequencies of 7.8 Hz and 15.7 Hz. Under the rotating frequency of 2.5 Hz, the VIV still exists. A new peak frequency of 2.5 Hz, the same as the rotating frequency, appears in the spectrum and it is considered that both the VIV and the whirl contribute to the cylindrical vibration response. A similar phenomenon is observed at a rotating frequency of 5 Hz, different from that at a rotating frequency of 2.5 Hz. The amplitude in the cross-flow direction dramatically increases (Fig. 12), which indicates that, with the increase of rotation frequency, the rotating frequency dramatically affects the vibration response at $U = 0.46$ m/s. At a rotating frequency of 7.5 Hz, the amplitude in the cross-flow direction seems to be limited due to the increased mean lift.

Fig. 13 shows the displacement time histories and motion trajectories of the middle of the rotating pipe at different rotation frequencies, with a flow velocity of 1.02 m/s. With the increase of rotation frequency, the time histories of the in-line and cross-flow displacement of the rotating pipe remain periodic. The trajectory gradually remains at the original figure '8' shape, and the direction of motion was opposite to the direction of rotation of the rotating pipe.

Fig. 14 shows the displacement spectrum in the middle of the rotating pipe at different rotation frequencies for $U = 1.02$ m/s. Without rotation, the vibration is mainly caused by VIV with dominant vibration frequencies of 12.4 Hz and 24.9 Hz. With an increase in rotation, the frequency of vibration in the in-line direction and in the cross-flow direction is not much different from that without rotation. The whirl component disappears and is considered to be suppressed by the VIV, resulting in little difference in amplitude, as shown in Fig. 15.

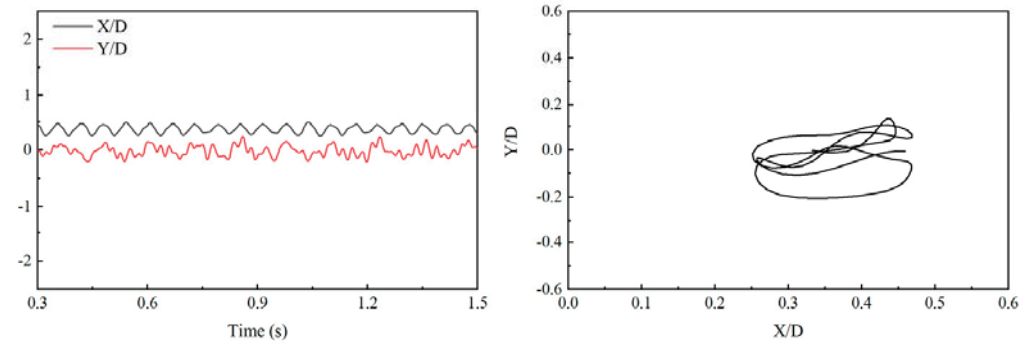

(*a*) $f = 0\,\mathrm{Hz}$

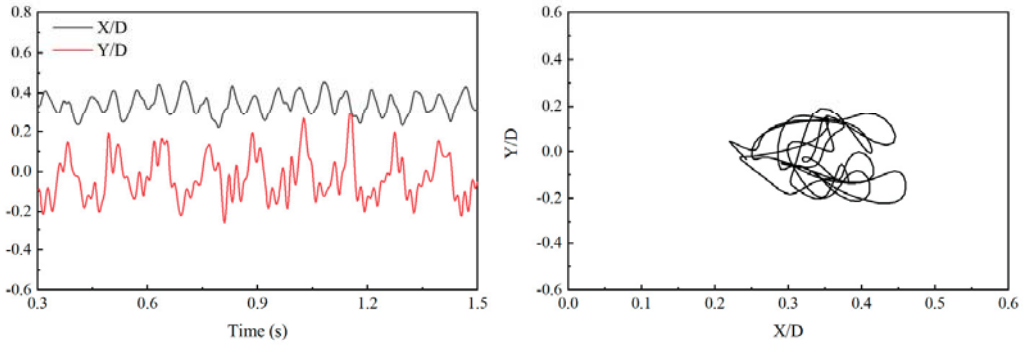

(*b*) $f = 2.5\,\mathrm{Hz}$

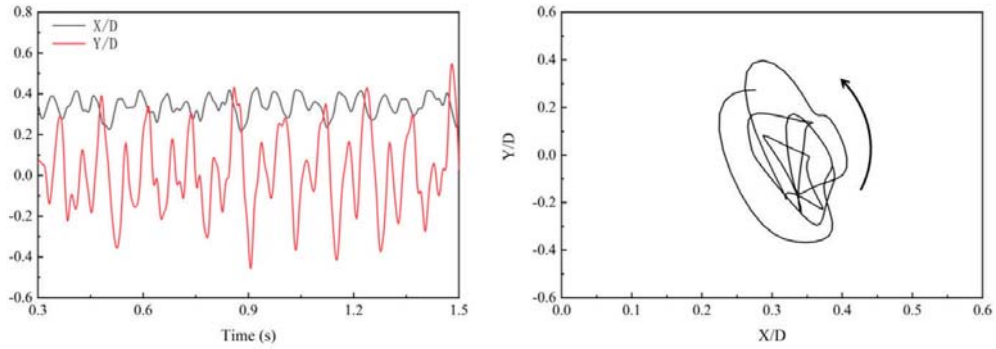

(*c*) $f = 5.0\,\mathrm{Hz}$

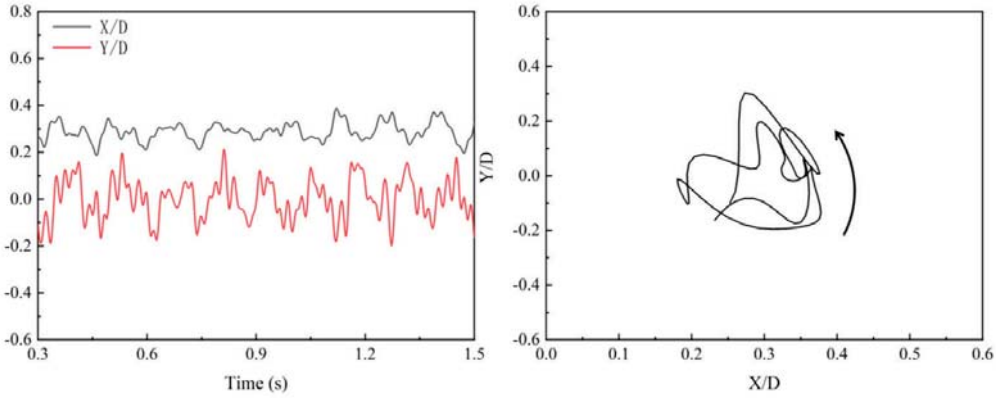

(*d*) $f = 7\,5\,\mathrm{Hz}$

Fig. 10. Time course histories of displacement and trajectories of the middle of the rotating pipe at different rotation frequencies for U=0.46 m/s

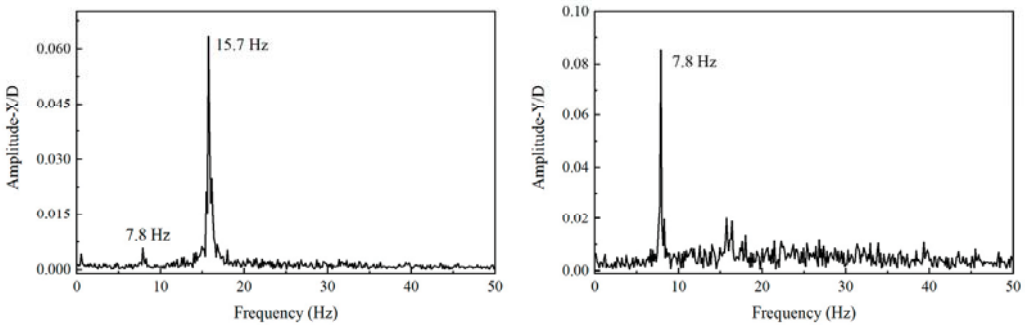

(*a*) $f = 0\,\mathrm{Hz}$

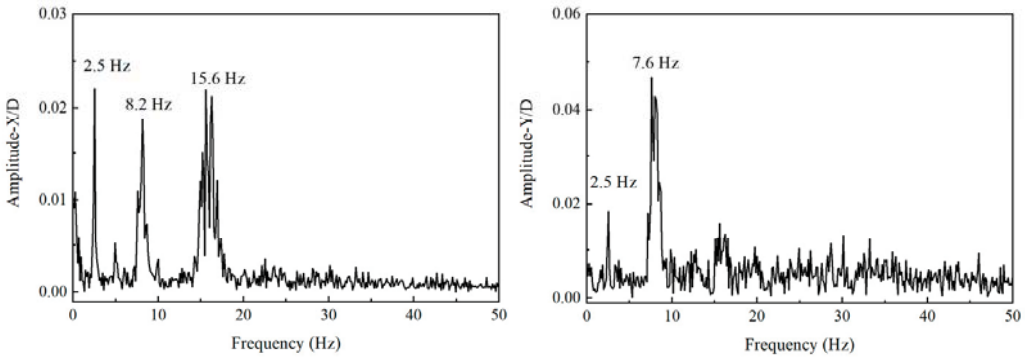

(*b*) $f = 2.5\,\mathrm{Hz}$

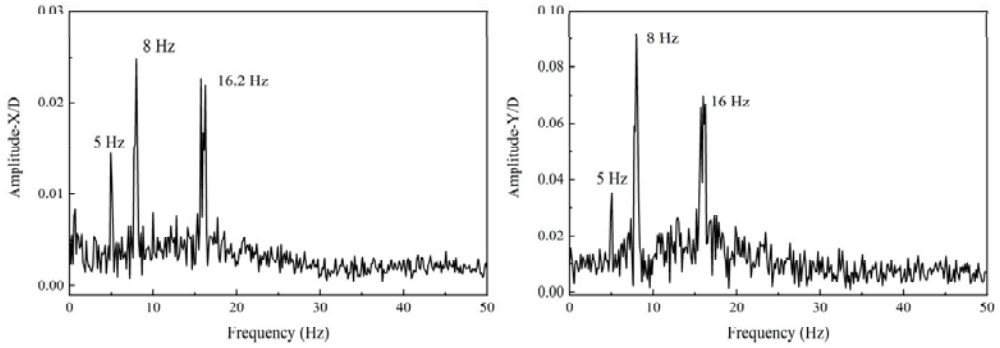

(*c*) $f = 5.0\,\mathrm{Hz}$

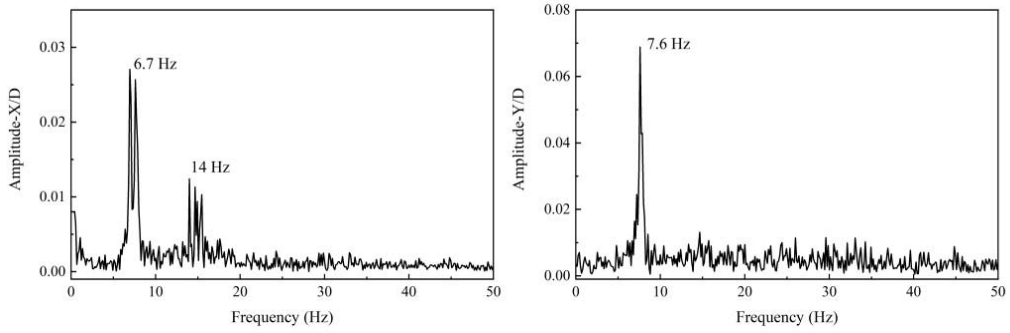

(*d*) $f = 7.5\,\mathrm{Hz}$

Fig. 11. Spectrum of displacement in the middle of the rotating pipe at different rotation frequencies for U=0.46 m/s

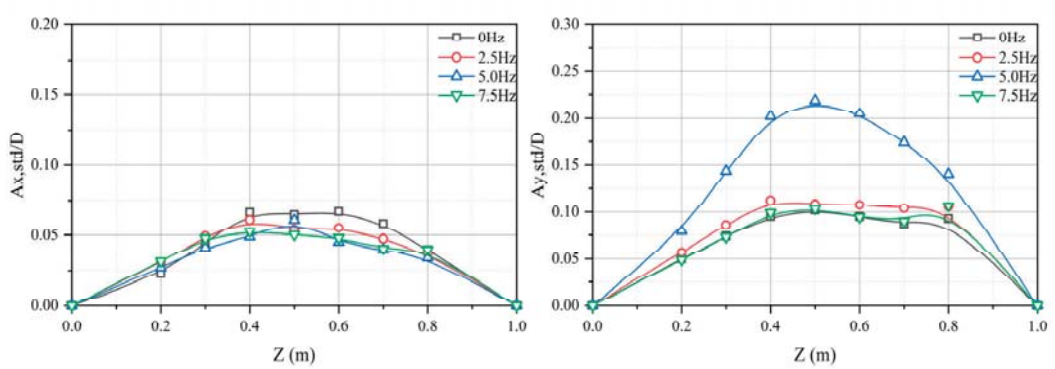

Fig. 12. RMS values of the cross-flow and cross-flow amplitudes of the rotating pipe at different rotating frequencies for U=0.46 m/s

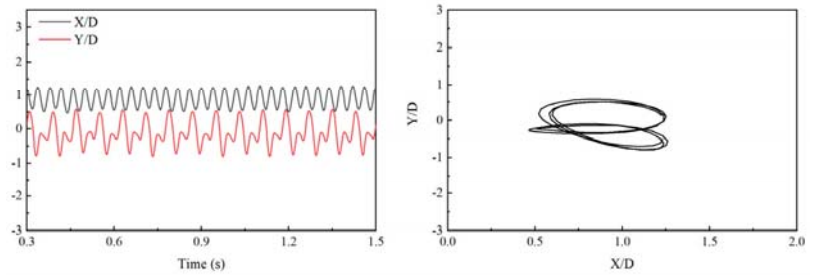

(*a*) $f = 0\,\mathrm{Hz}$

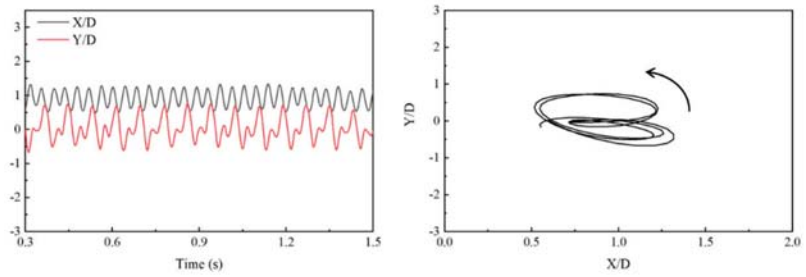

(*b*) $f = 2.5\,\mathrm{Hz}$

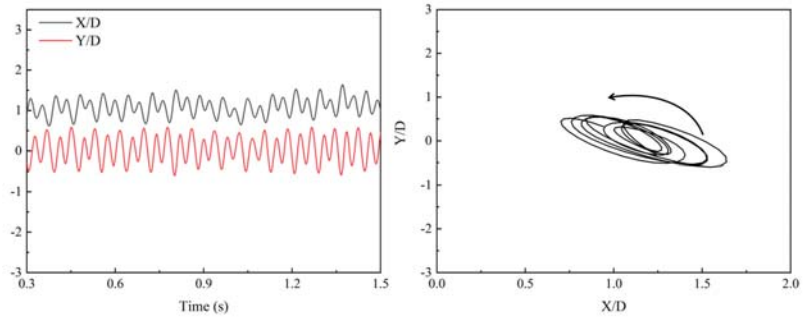

(*c*) $f = 5.0\,\mathrm{Hz}$

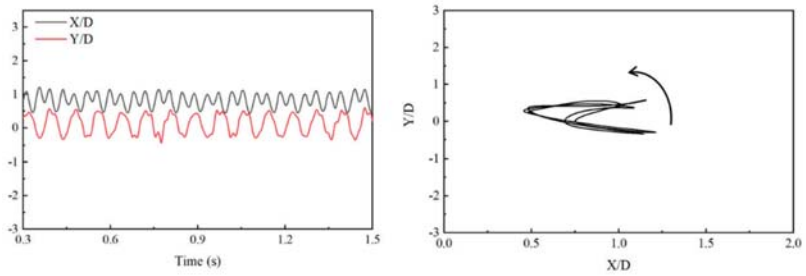

(*d*) $f = 7.5\,\mathrm{Hz}$

Fig. 13. Time course histories of displacement and trajectories of the middle of the rotating pipe at different rotation frequencies for U= 1.02 m/s

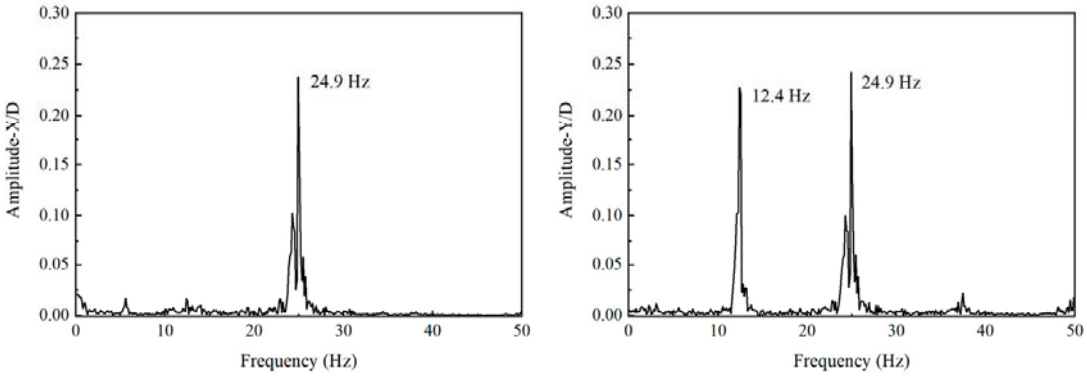

(*a*) $f = 0\,\mathrm{Hz}$

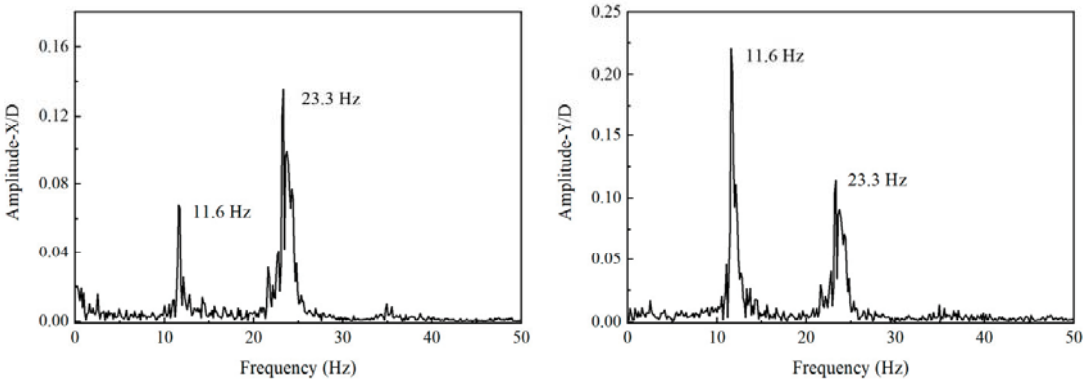

(*b*) $f = 2.5\,\mathrm{Hz}$

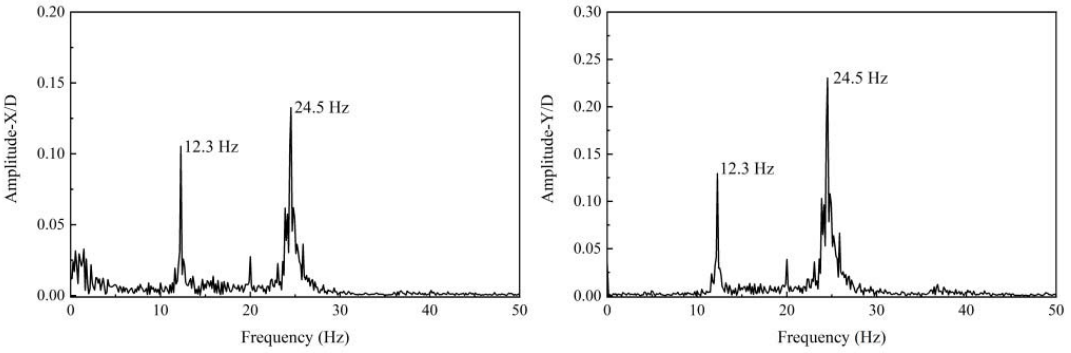

(*c*) $f = 5.0\,\mathrm{Hz}$

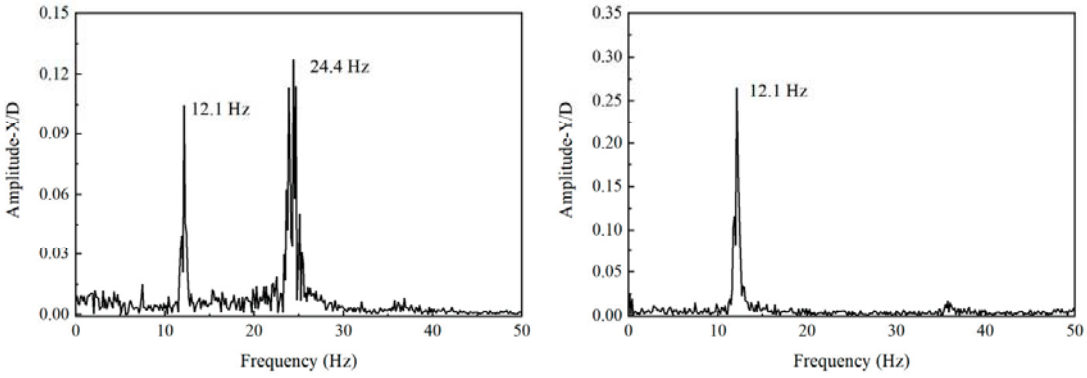

(*d*) $f = 7\,5\,\mathrm{Hz}$

Fig. 14. Spectrum of displacement in the middle of the rotating pipe at different rotation frequencies for U= 1.02 m/s

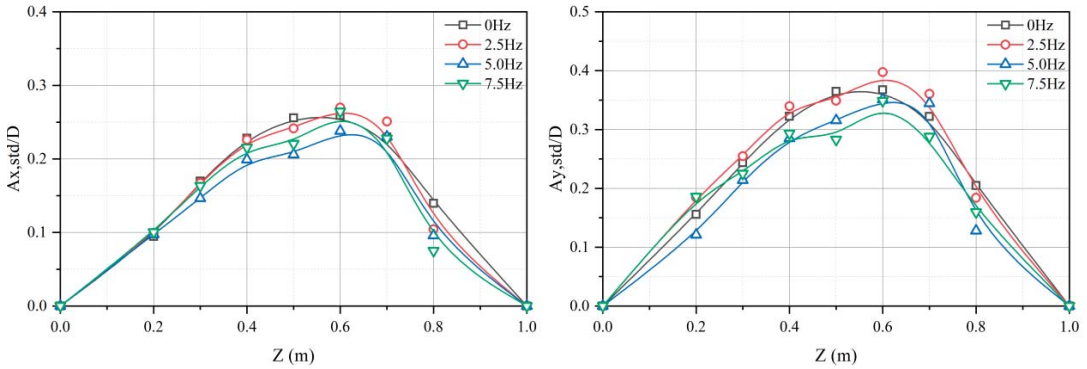

Fig. 15. RMS values of the cross-flow and cross-flow amplitudes of the rotating pipe at different rotating frequencies for U= 1.02 m/s

VIBRATION RESPONSE WITH REDUCED VELOCITY

Based on the displacement and frequency response of the rotating pipe, the variation in the transverse vibration frequency ratio and relative amplitude, with the reduced velocity of the rotating pipe, was analysed further. The vibration frequency ratio is $f^* = f_v / f_n$ and the relative amplitude is $A^* = A / D$. Fig. 16 shows the variation of the cross-flow relative amplitude to frequency ratio response of the rotating pipe with the flow velocity at different rotation frequencies. Consistent with the previous section, the velocity U= 1.02 m/s is within the locking interval of the natural frequency and the amplitude dramatically increases. At flow velocities of U= 0.72 m/s and U= 1.02 m/s, the rotating pipe is dominated by the VIV and has similar amplitudes at the different rotation frequencies. However, at a flow velocity of U= 0.46 m/s, the rotating pipe is dominated by the VIV and whirl, and the rotation affects the vibration response.

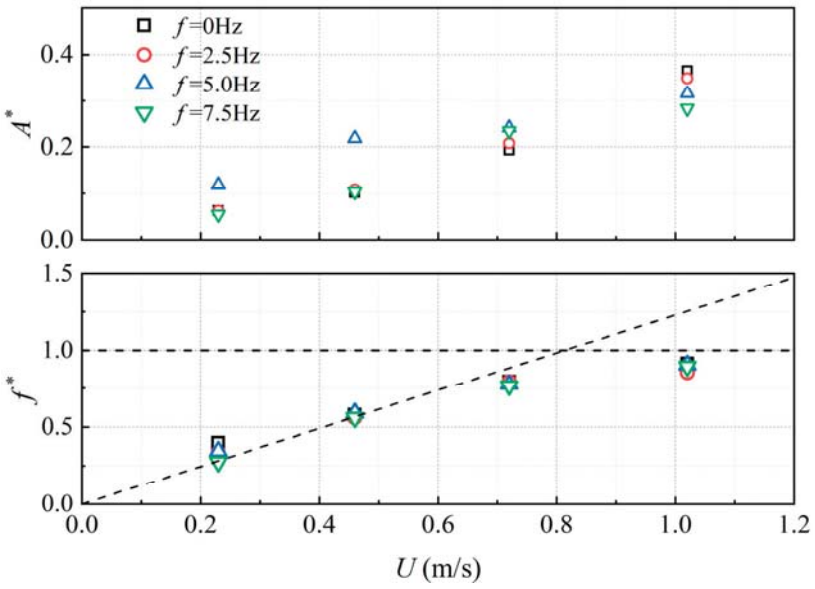

Fig. 16. Variation of relative amplitude to frequency ratio with reduced velocity in the cross-flow direction of the rotating pipe at different rotation frequencies

CONCLUSIONS

In this paper, experiments on in flow rotating pipe vibrations were conducted at rotation frequencies of f = 0.0 Hz, 2.5 Hz, 5.0 Hz, and 7.5 Hz and flow velocities U = 0 m/s, 0.46 m/s, 0.72 m/s, and 1.02 m/s. The experimental data were processed by the image tracking method and the flow vibration characteristics of the rotating pipe were in flow and rotation. The main conclusions are:

(1) For a pipe in flow without rotation, the vibration of the pipe is mainly caused by the vortex shedding, twice the frequency component of the vibration in the cross-flow direction can be obtained and the trajectory diagram is '8' shaped. For a rotating pipe in static water, with an increase in rotating frequency, multiple frequency components are generated, the motion gradually becomes an inclined circle, and 'positive direction whirl' is generated.

(2) The variation of the cross-flow's relative amplitude to frequency ratio response of the rotating pipe at different rotation frequencies is related to the vibration mode of the rotating pipeline and is influenced by the flow velocity. The variation of the cross-flow's relative amplitude to frequency ratio response of the rotating pipe with the flow velocity at different rotation frequencies. The velocity U= 1.02 m/s is within the locking interval of the natural frequency and the amplitude dramatically increases. At flow velocities of U= 0.72 m/s and U= 1.02 m/s, the rotating pipe is dominated by the VIV and there is not much difference in amplitude at different rotation frequencies.

(3) For a rotating pipe in flow (at a flow velocity of U= 0.46 m/s), with an increase in rotation frequency, 'reverse direction whirl' is generated. The vibration seems to be dominated by the combination of VIV and the whirl. At flow velocities of U= 0.72 m/s and U= 1.02 m/s, the whirl seems to be suppressed and the vibration is considered to mainly be dominated by the VIV.

DECLARATION OF COMPETING INTEREST

The authors declare that they have no known competing financial interests or personal relationships that could have appeared to influence this work.

ACKNOWLEDGEMENTS

This work was supported by the Natural Science Foundation of Hubei Province (2021CFB064), the National Natural Science Foundation of China (52201334) and the open fund of the State Key Laboratory of Coastal and Offshore Engineering (LP2203). The authors are very grateful to the referees for their helpful comments and suggestions, which helped to improve this paper.

REFERENCES

1. M. J. Moharrami, C. de Arruda Martins, and H. Shiri, "Nonlinear integrated dynamic analysis of drill strings under stick-slip vibration," Applied Ocean Research, vol. 108, p. 102521, 2021. doi:https://doi.org/10.1016/j.apor.2020.102521.

2. R. Wang, X. Liu, G. Song, and S. Zhou, "Non-Linear Dynamic Analysis of Drill String System with Fluid-Structure Interaction," Applied Sciences, vol. 11, p. 9047, 2021. doi:https://doi.org/10.3390/app11199047.

3. M. Stosiak, M. Zawiślak, and B. Nishta, "Studies of resistances of natural liquid flow in helical and curved pipes," in Proceedings of the 14th International Scientific Conference: Computer Aided Engineering, pp. 759-766, 2019. dio:https://doi.org/10.2478/pomr-2018-0103.

4. A. Ghasemloonia, D. G. Rideout, and S. D. Butt, "A review of drillstring vibration modeling and suppression methods," Journal of Petroleum Science and Engineering, vol. 131, pp. 150-164, 2015. doi:https://doi.org/10.1016/j.petrol.2015.04.030.

5. F. Liang, X.-D. Yang, W. Zhang, and Y.-J. Qian, "Vibrations in 3D space of a spinning supported pipe exposed to internal and external annular flows," Journal of Fluids and Structures, vol. 87, pp. 247-262, 2019. doi:https://doi.org/10.1016/j.jfluidstructs.2019.04.002.

6. F. Wang and N. Chen, "Dynamic response analysis of drill pipe considering horizontal movement of platform during installation of subsea production tree," Polish Maritime Research, 2020. doi:https://doi.org/10.2478/pomr-2020-0043.

7. G. Gao, Y. Cui, and X. Qiu, "Prediction of vortex-induced vibration response of deep sea top-tensioned riser in sheared flow considering parametric excitations," Polish Maritime Research, 2020. doi:https://doi.org/10.2478/pomr-2020-0026.

8. P. Catalano, M. Wang, G. Iaccarino, and P. Moin, "Numerical simulation of the flow around a circular cylinder at high Reynolds numbers," International Journal of Heat and Fluid Flow, vol. 24, pp. 463-469, 2003. doi:https://doi.org/10.1016/S0142-727X(03)00061-4.

9. D. Stojković, M. Breuer, and F. Durst, "Effect of high rotation rates on the laminar flow around a circular cylinder," Physics of Fluids, vol. 14, pp. 3160-3178, 2002. doi:https://doi.org/10.1063/1.1492811.

10. M. H. Chou, "Numerical study of vortex shedding from a rotating cylinder immersed in a uniform flow field," International Journal for Numerical Methods in Fluids, vol. 32, pp. 545-567, 2000. doi:https://doi.org/10.1002/(SICI)1097-0363(20000315)32:5<545::AID-FLD948>3.0.CO;2-2.

11. R. K. Ray and J. C. Kalita, "Higher-order-compact simulation of unsteady flow past a rotating cylinder at moderate Reynolds numbers," Computational and Applied Mathematics, vol. 35, pp. 219-250, 2016. doi:https://doi.org/10.1007/s40314-014-0191-2.

12. M. J. Ezadi Yazdi, A. S. Rad, and A. B. Khoshnevis, "Features of the flow over a rotating circular cylinder at different spin ratios and Reynolds numbers: Experimental and numerical study," The European Physical Journal Plus, vol. 134, pp. 1-21, 2019. doi:https://doi.org/10.1140/epjp/i2019-12508-3.

13. Y. Chew, M. Cheng, and S. Luo, "A numerical study of flow past a rotating circular cylinder using a hybrid vortex scheme," Journal of Fluid Mechanics, vol. 299, pp. 35-71, 1995. doi:https://doi.org/10.1017/S0022112095003417.

14. D. Stojković, P. Schön, M. Breuer, and F. Durst, "On the new vortex shedding mode past a rotating circular cylinder," Physics of Fluids, vol. 15, pp. 1257-1260, 2003. doi:https://doi.org/10.1063/1.1562940.

15. J. O. Pralits, L. Brandt, and F. Giannetti, "Instability and sensitivity of the flow around a rotating circular cylinder," Journal of Fluid Mechanics, vol. 650, pp. 513-536, 2010. doi:https://doi.org/10.1017/S0022112009993764.

16. J. O. Pralits, F. Giannetti, and L. Brandt, "Three-dimensional instability of the flow around a rotating circular cylinder," Journal of Fluid Mechanics, vol. 730, pp. 5-18, 2013. doi:https://doi.org/10.1017/jfm.2013.334.

17. J. Meena and S. Mittal, "Three-dimensional flow past a rotating cylinder," Journal of Fluid Mechanics, vol. 766, pp. 28-53, 2015. doi:https://doi.org/10.1017/jfm.2015.6.

18. L. Ding, H. Kong, Q. Zou, J. Wang, and L. Zhang, "2-DOF vortex-induced vibration of rotating circular cylinder in shear flow," Ocean Engineering, vol. 249, p. 111003, 2022. doi:https://doi.org/10.1016/j.oceaneng.2022.111003.

19. Q. Zou, L. Ding, H. Wang, J. Wang, and L. Zhang, "Two-degree-of-freedom flow-induced vibration of a rotating circular cylinder," Ocean Engineering, vol. 191, p. 106505, 2019. doi:https://doi.org/10.1016/j.oceaneng.2019.106505.

20. Q. Zou, L. Ding, R. Zou, H. Kong, H. Wang, and L. Zhang, "Two-degree-of-freedom flow-induced vibration of two circular cylinders with constraint for different arrangements," Ocean Engineering, vol. 225, p. 108806, 2021. doi:https://doi.org/10.1016/j.oceaneng.2021.108806.

21. A. Munir, M. Zhao, H. Wu, L. Lu, and D. Ning, "Three-dimensional numerical investigation of vortex-induced vibration of a rotating circular cylinder in uniform flow," Physics of Fluids, vol. 30, p. 053602, 2018. doi:https://doi.org/10.1063/1.5025238.

22. A. Munir, M. Zhao, H. Wu, and L. Lu, "Numerical investigation of wake flow regimes behind a high-speed rotating circular cylinder in steady flow," Journal of Fluid Mechanics, vol. 878, pp. 875-906, 2019. doi:https://doi.org/10.1017/jfm.2019.677.

23. T. Tang, H. Zhu, J. Song, B. Ma, and T. Zhou, "The state-of-the-art review on the wake alteration of a rotating cylinder and the associated interaction with flow-induced vibration," Ocean Engineering, vol. 254, p. 111340, 2022. doi:https://doi.org/10.1016/j.oceaneng.2022.111340.

24. J. Zhao, D. L. Jacono, J. Sheridan, K. Hourigan, and M. C. Thompson, "Experimental investigation of in-line flow-induced vibration of a rotating circular cylinder," Journal of Fluid Mechanics, vol. 847, pp. 664-699, 2018. doi:https://doi.org/10.1017/jfm.2018.357.

25. K. W. L. Wong, J. Zhao, D. L. Jacono, M. C. Thompson, and J. Sheridan, "Experimental investigation of flow-induced vibration of a sinusoidally rotating circular cylinder," Journal of Fluid Mechanics, vol. 848, pp. 430-466, 2018. doi:https://doi.org/10.1017/jfm.2018.379.

26. R. Bourguet, "Flow-induced vibrations of a rotating cylinder in an arbitrary direction," Journal of Fluid Mechanics, vol. 860, pp. 739-766, 2019. doi:https://doi.org/10.1017/jfm.2018.896.

27. R. Bourguet, "Two-degree-of-freedom flow-induced vibrations of a rotating cylinder," Journal of Fluid Mechanics, vol. 897, 2020. doi:https://doi.org/10.1017/jfm.2020.403.

28. R. Bourguet and D. L. Jacono, "Flow-induced vibrations of a rotating cylinder," Journal of Fluid Mechanics, vol. 740, pp. 342-380, 2014. doi:https://doi.org/10.1017/jfm.2013.665.

29. K. H. Aronsen, "An experimental investigation of in-line and combined in-line and cross-flow vortex induced vibrations," 2007. doi:10.1115/1.4038350.

30. W. Chen, C.-k. Rheem, X. Li, and Y. Lin, "Investigation of the motion characteristics for a spring-mounted rotating cylinder in flow," Journal of Marine Science and Technology, vol. 25, pp. 1228-1245, 2020. doi:https://doi.org/10.1007/s00773-020-00711-y.